Austempering Ce-La inoculated solution strengthened ferritic ductile cast irons

Serdar Osman Yılmaz[1], Tanju Teker[2]*, Demet Demir[3]

[1,3]*Tekirdağ Namık Kemal University, Faculty of Engineering, Department of Mechanical Engineering, 59860, Çorlu, Tekirdağ, Turkey*
[2]*Sivas Cumhuriyet University, Faculty of Technology, Department of Manufacturing Engineering, 58140, Sivas, Turkey*

Abstract

The influence of austempering conditions on the microstructure, hardness, tensile strength, and impact toughness of Ce-La inoculated solution-strengthened ferritic ductile irons was analyzed. The austempering was performed at temperatures 280, 320, 420, 520, and 620 °C for periods of 1.5 and 2.5 h. Metallurgical characterization of the samples was determined using scanning electron microscopy, optical microscopy, X-ray diffraction, microhardness, impact, and tensile test. The fracture surfaces of the tensile samples were examined by scanning electron microscopy. Austempering heat treatment significantly enhanced the mechanical characteristics of solution-strengthened ferritic ductile cast iron. This led to the birth of solution-strengthened Ce-La inoculated ferritic cast iron, a new spheroidal graphite cast iron family member with a unique microstructure in an ausferritic matrix. Samples austempered for low temperature exhibited higher impact toughness and tensile strength due to the nano-sized ausferrite phase. Austempering for high temperatures displayed higher elongation.

K e y w o r d s: austempering, ausferrite, hardness, impact test

1. Introduction

The solution-strengthened ferritic ductile cast iron (SSFDCI) has a spherical graphite embedded in a ferritic matrix, and ausferrite and acicular ferrite phases can form in the microstructure after heat treatment [1, 2]. The matrix structure surrounding the free graphite nodules is designed to produce a microstructure having carbide-free ferrite (ausferrite) phases depending on the isothermal heat treatment conditions. SSFDCI has some advantages like lower density than forged steel, such as better vibration, developed lubrication features, lower raw material costs, significant energy savings during production for specific components, approximately two times stronger than pearlitic ductile cast iron, high elongation, and toughness [3–4]. There is no pre-eutectoid ferrite in the ADI matrix processed by conventional austempering. The very low content of converted ferrite (α) also limits ductility. In order to improve the machinability and ductility of ADI, the issue of producing ADI with pre-eutectoid ferrite

and ausferrite structures has gained great importance. This can be achieved by austempering [5–7]. The upper and lower austempering temperatures of DCI are related to the chemical composition of the alloy. Austempering will produce a unique microstructure of pre-eutectoid ferrite, ausferrite, and carbon-enriched austenite. This material is expected to exhibit much greater ductility than conventionally quenched and tempered ductile iron. The tensile and yield strengths of this material will be higher than those of pearlitic types. This critical heat treatment process will also increase machinability in ADI. The austenitizing process is an important part of the austempering heat treatment. Iron alloys are used to produce the austenite phase before the matrix transforms into ausferrite [8–10]. Austempering conditions also define the final carbon content, which determines the ratio and size of the ausferrite phases. This determines the optimum strength-elongation ratio. Austempering is applied as a two-stage process, in which the first stage is the austenitization stage in the temperature range of 815–

*Corresponding author: tel.: +90 346 2191241; e-mail address: tanjuteker@cumhuriyet.edu.tr

T a b l e 1. Chemical content of test samples (wt.%)

	Fe	C	Si	Mn	P	S	Cr	Cu	Ce-La	Mg	Al	Ti	Other
S1–S11	91.136	3.10	4.30	0.24	0.025	0.025	0.020	0.07	0.12	0.048	0.007	0.017	Bal.
S12	91.093	3.12	4.29	0.27	0.025	0.025	0.014	0.09	–	0.052	0.009	0.012	Bal.

T a b l e 2. The experimental parameters for solution-strengthened ferritic ductile irons

Sample no.	Austenitizing temperature (°C)	Austenitizing time (h)	Quench medium	Austempering temperature (°C)	Austempering time (h)	Quenching
S1-Ref.	As-cast	–	–	–	–	–
S2	900	1	Salt	280	1.5	Air
S3	900	1	Salt	280	2.5	Air
S4	900	1	Salt	320	1.5	Air
S5	900	1	Salt	320	2.5	Air
S6	900	1	Salt	420	1.5	Air
S7	900	1	Salt	420	2.5	Air
S8	900	1	Salt	520	1.5	Air
S9	900	1	Salt	520	2.5	Air
S10	900	1	Salt	620	1.5	Air
S11	900	1	Salt	620	2.5	Air
S12	900	1	Salt	280	1.5	Air

920 °C for 1 to 4 h. The specific austenitization temperature selected is related to the subsequent austempering temperature of DI. A rapid quenching follows the austenitization stage in a salt bath in which the castings are kept isothermally at the chosen austempering temperature, usually in the range of 230–450 °C according to the required properties of castings. Due to the high strength obtained by increasing the Si content of SSFDCI by more than 3.8 wt.%, it represents more attractive mechanical properties than pearlitic kind ductile cast irons [11–13]. The idea is to have a solution-strengthened structure by the interstitial atoms in the crystal lattice of the parent metal. In this crystalline system, the elements can be arranged as a substitute solid solution or an interstitial solid solution depending on the size of the alloy element. Carbon in iron is a good example of this solid solution structure. In the interstitial solution, interstitial atoms are caused to compress and thus deform the bonds of the original atoms. Both types mainly cause strengthening by local tension, which limits the movement of the dislocations and strengthens the material. It is recommended to strengthen the ferritic structure with silicon [14, 15]. Soivio reported that the separation of silicon reduces the solubility of carbon near the graphite nodules in the Si solution-reinforced matrix and also reduces the stability and impairs the workability of the carbon-stabilized austenite [16].

This study aims to analyze the influence of austempering conditions on the microstructure, hardness, tensile strength, and toughness grades of Ce-La inoc-

ulated solution-strengthened ferritic ductile cast irons (SSFDCI).

2. Materials and method

The chemical content of the samples used in the experiments is given in Table 1. Melting was applied in an induction furnace of 300 kg using steel scrap. The melts were heated at 1510 °C with an induction furnace, and alloying elements were added to the induction furnace. The Ce-La modifier included 65 % Ce and 30 % La and was added about "0.1 wt.%" to the inoculation with foundriSil (Si-Ba-Ca-Al) containing 75 wt.% Si with Elkem Wear Seed. 5 % Magnesium – 42 % FeSi (SNAM MG 6811) treatment in the crucible was conducted via the sandwich method. Y-block molds were done by ASTM standard A571M, as illustrated in Fig. 1 [17].

The prepared melt was transferred to the casting pot at 1460 °C. Experimental parameters of austempered solution strengthened ferritic ductile iron are given in Table 2. Austempering was a heat operation implemented in two stages. In the initial stage of the process, samples were austenitized. In the second stage of the process, the austenitized samples were austempered by isothermal annealing. For this goal, samples were austenitized at 900 °C for 1.5 h, then transferred to a fixed heat salt bath for austempering, and held at this temperature for 1.5 and 2.5 h. It was then cooled to room temperature to finish the austempering pro-
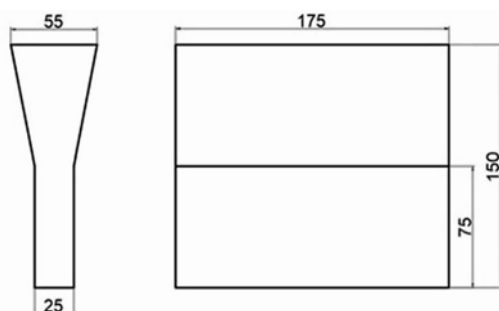
Fig. 1. Illustration of Y-block mold.

cess, and the cooling rate was applied as $25–100\,°C\,s^{-1}$. Austenitization was carried out in a Protherm furnace. Samples were covered in graphite powder. Austempering was applied at temperatures 280, 320, 420, 520, and 620 °C. The salt bath was created by placing a stainless-steel crucible in a Protherm vertical furnace and embedding the heat treatment salt in the crucible. Then, final polishing was performed on the polisher disc device using a 2 μm diamond solution. Samples were etched by immersion in the nital solution for metallographic examination. The microstructural investigations were carried out using scanning electron microscopy (SEM) and optical microscopy (OM). X-ray diffraction (XRD) analysis was performed using Cu-α radiation at 40 kV and 100 mA to observe the phase content. The elemental contents of the samples were examined by energy distribution spectrometry (EDS). Microhardness analysis was performed using a 100 g load at 0.5 mm intervals on the Vickers scale on the Qness Q10 microhardness testing machine. Tensile test samples were done according to ASTM E8M–04 standards. Tests were performed with a 100 kN Instron test system [18]. Charpy impact samples were prepared according to ASTM E23–06 standards. Impact tests were conducted at –40/+40 °C temperature intervals [19]. The fracture surfaces of the tensile samples were examined by SEM.

3. Results and discussion

3.1. Evaluation of metallurgical structure

The SEM micrograph of the cast sample is given in Fig. 2. The casting microstructure indicated an effective ferritic matrix with nearly 2 % pearlite.

Figure 3 shows SEM micrographs of S2, S4, S6, S8, and S10 samples austenitized at 900 °C and austempered for 280, 320, 420, 520, and 620 °C with a fixed austempering time of 1.5 h. Two phases were determined in the matrix of the austempered sample. In the microstructure, needle-shaped dark-colored ausferrite and residual austenite were detected. The di-
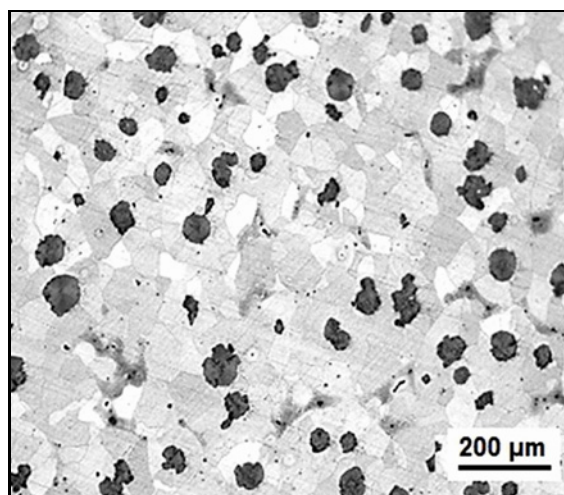

Fig. 2. SEM micrograph of as-cast structure.

rections of ausferrite laths at lower conversion temperatures were non-uniform and thinner. When the subcritical temperature was raised from 320 to 420 °C, the ausferrite laths expanded, and austenite was retained between adjacent ferrite forming ausferrite and thicknesses enriched with carbon. It is thought that in the first phase of the conversion, ferrite nucleated at the austenite grain boundary and expanded in parallel plates or laths by the refusal of carbon to austenite, where ausferrite and ferrite appeared in the microstructure of the samples. The ausferrite that occurred at the beginning of the transformation might have had maximum lateral growth, and it was enclosed by a ferrite with a smaller carbon amount [20]. The rise in the carbon rate of austenite resulted from ferrite dissolution, which decreased the incentive force for the sideways growth of the ausferrite in the final step of conversion [21]. Microstructural observations showed that the austempering temperature slightly modified the ausferrite length, and the width showed a significant difference with the austempering temperature.

Figure 3 indicates the ausferrite bulk fraction and size as a role of the austempering situations. Samples are given in Fig. 3 for the 280–620 °C range. After transformation over 320 °C, retained austenite formed mainly as interlath films in the structure (Figs. 3d,e) for heat treatment periods. Ausferrite formed as great pools after partial conversion of the austenite for the sample S12 without Ce inoculation (Figs. 3a,f). The ferrite plates separated from each other in particular of ausferrite, and distinctions in ausferrite fraction on microstructures produced at 320/420 °C significantly impacted the dispersion of this phase due to the presence of Ce-La (Figs. 3c,f). It is seen that ausferrite did not form homogeneously in the matrix without cerium inoculation (Fig. 3f). Figure 4 shows SEM micrographs of samples S5, S7, and S9. For long
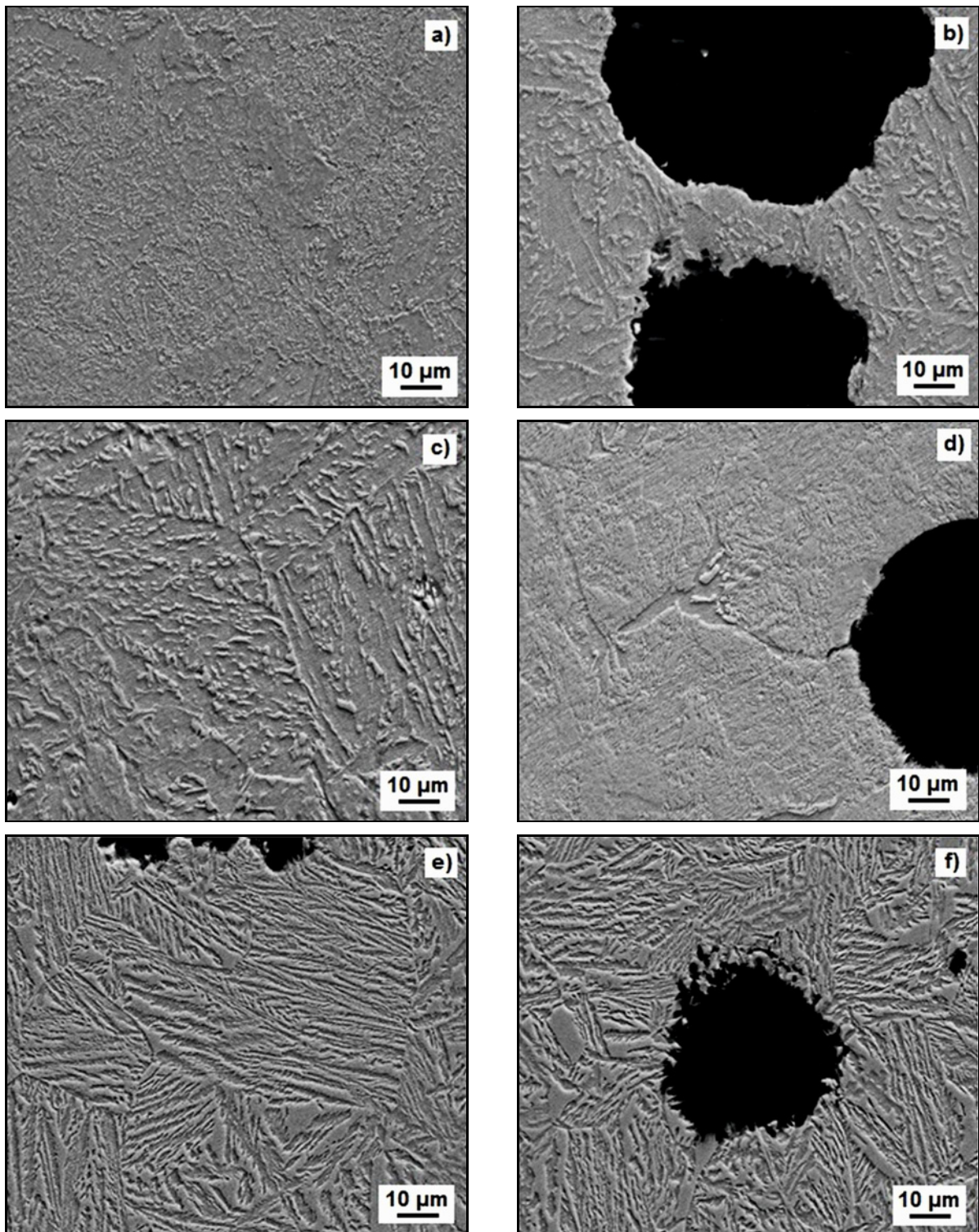
Fig. 3. SEM micrographs of samples: (a) S2, (b) S4, (c) S6, (d) S8, (e) S10, and (f) S12.

(2.5 h) austempering times at 280 °C, the structure was almost the same as established for the austempering time of 1.5 h (Fig. 4a). Precise austenite dissociation to ferrite and ausferrite at higher temperature (320–520 °C) was noticed (Figs. 4b,d). A considerable reduction in the ferrite bulk fraction could not be appraised over 280 °C, and alone ausferrite occurred in the fine foils due to increased austempering time to 2.5 h. To prevent confusion due to the prior occurrence of martensite, the samples were processed at 280–520 °C for 2.5 h without any indication of this phase formed before austempering (Fig. 4). It

Fig. 4. SEM micrographs of samples: (a) as-cast, (b) S5, (c) S7, and (d) S9.

is seen that increasing the austempering time to 2.5 h forms nano-sized ausferrite. EDS analysis of the as-cast sample is presented in Fig. 5. C, Fe, Si, Mn, and S were the parent elements of the as-cast sample. The microstructure of SSFDCI mainly contained a mixture of graphite and ferrite. This specific product of austempering heat treatment is named "ausferrite" [23, 24]. Ferrite was available in a needle-shaped, acicular form and was stabilized by austenite carbon; hence it was also called high-carbon austenite. This ausferritic structure was obtained pending the special austempering heat treatment. Short cast diffusion may form when cast iron is austempered below 420 °C, and carbon replaces ferrite as it accumulates in austenite [23]. This reaction probably lets the carbon rate in austenite increase up to 2 wt.%, stabilize the austenite, and fine acicular ferrite in the austenite matrix creates further strength and toughness. Austempering time is an important factor affecting the phase transition of the SSFDCI produced, where austempering time increased from 1.5 to 2.5 h ausferrite thickened, nano-sized austenite dispersed (Fig. 4).

Austenited microstructures indicated a dark needle-like ferrite and a brightly etched dispersed austenite with scattered graphite nodules after austempering at various temperatures for 2.5 h. Ferrite gradually increased as the austempering temperature rose from 420 to 520 °C. With the austempering temperature rising to 480 °C, ausferrrite showed plate-like morphology for 1.5 h austempering. On the other hand, the increase of austempering time dispersed austenite in the matrix homogeneously. Increasing austempering time also caused large ferritic needles. A higher nucleation rate at a lower time produced many fine ferrite needles due to excessive supercooling. The lower nucleation rate resulted in fewer ferrite needles that reached a wider size at a higher time. The effect of austempering temperature on SSFDCI samples was analyzed, and the nodularity of conventional SSFDCI with austempered SSFDCI was checked. Figures 3 and 4 show that there was no distinction in nodule properties. The number, size, distribution, and nodularity of the graphite patches were not affected by austempering processes and were only affected by melting
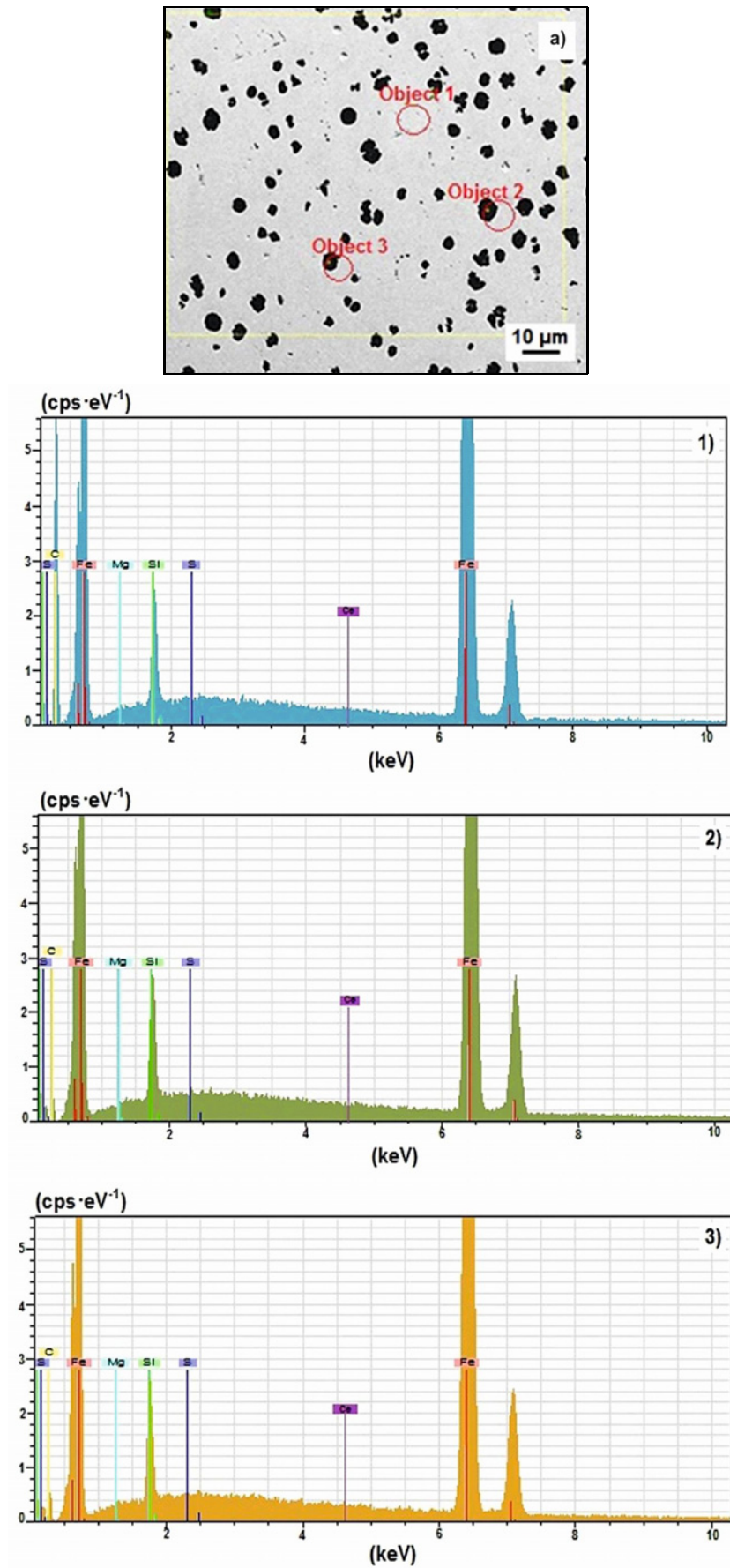
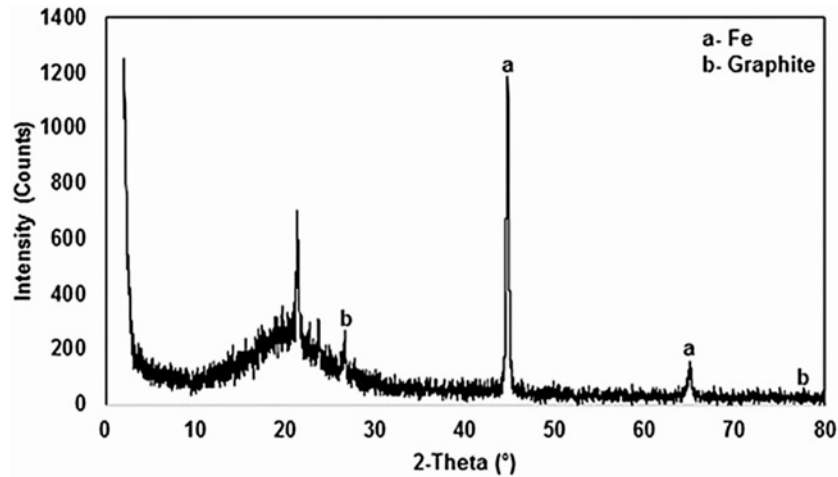Fig. 5. EDS analysis of as-cast sample.

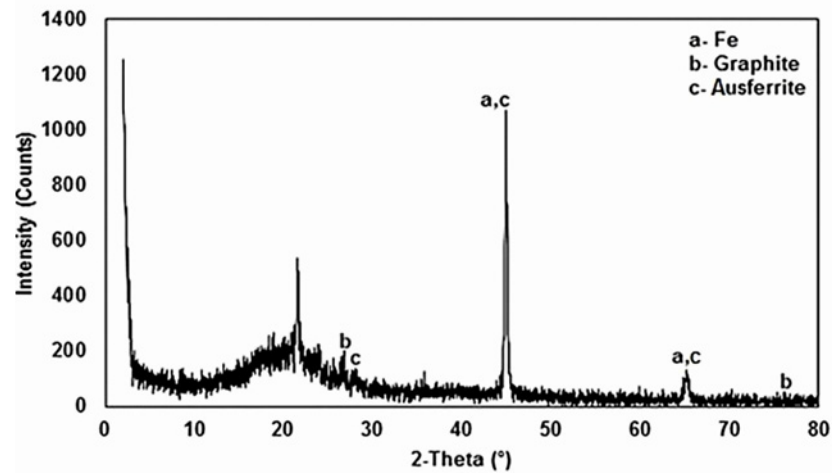Fig. 6. X-Ray pattern of as-cast sample.

Fig. 7. X-Ray pattern of S4 sample.

and casting applications [17–20]. Figure 4 reveals the graphite nodules placed in a ferritic matrix in the sample austempered for 280 °C for 1.5 h formed ausferrite, and an increase of austempering temperature produced 5–20 μm sized ausferrite. When the austempering time rose to 2.5 h, carbon-rich austenite dispersed in the microstructure. The samples austempered at 280 °C exhibited a typical less ausferrite microstructure with an acicular sight of ausferrite. In the ferrite matrix, an acicular appearance of ausferrite occurred after austempering at 320 °C (Fig. 4c). In Fig. 4, a plate-like morphology of ausferrite with higher rates of ausferrite at higher action temperature was detected. It was found that the presence of martensite was not determined for more than 1.5 h of austempering time, only ausferrite was present in the structure, and austenite was preserved (Fig. 4). This could be described by the fact that the carbon ratio was deficient in continuing the austenite stability in a minimum austempering time [23, 24]. However,

carbon abundance was adequate to stabilize austenite even after air cooling at excessive austempering times. Silicon inhibited the creation of cementite during ausferrite conversion for 2.5 h austempering. Ausferrite promoted the generation of carbon-enhanced austenite after local conversion. The existing high-carbon austenite had not been turned into martensite. The steady of the retained austenite depended on the high carbon and manganese rate in the alloy [18]. When a little of the austenite next to the grain boundaries was quenched in a salt bath at 420 °C, it first turned into ausferrite (Fig. 4c). The resulting ausferrite formed by residual austenite enriched with carbon. When cooled to room temperature, some of the austenite was probably preserved, and the residual turned into ausferrite (Figs. 6–8). The austenite retained in the existing isothermal converted samples was lesser in dimensions. Silicon was thought to stabilize the captured austenite by saturating the carbon content in an austempered structure. Acicular ferrite could also be seen at
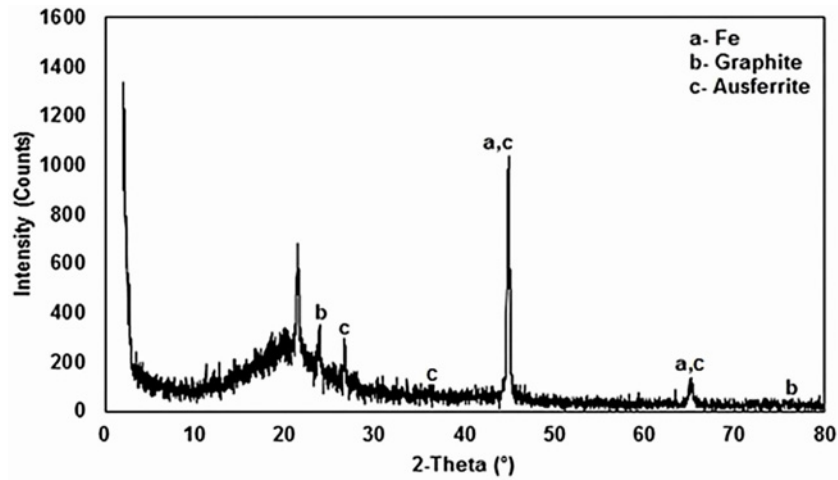
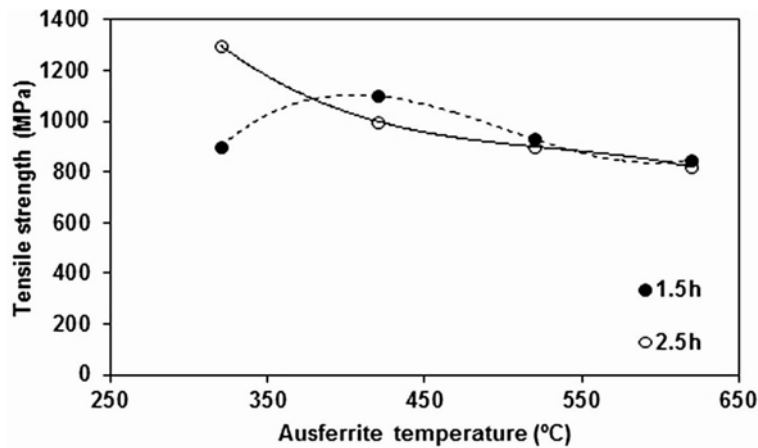Fig. 8. X-Ray pattern of S7 sample.

Fig. 9. The tensile test results of as-cast and austempered samples.

higher austempering temperatures. The average lath and acicular ferrite length were equal, and their thickness was different, and the morphology at the early phase of transformation was quite acicular and varied to the lath-like morphology because of lateral growth, as declared in austenitic ductile iron works [20].

The ferrite structure was nucleated and turned into ausferrite for high austempering temperatures. It manufactured thinner large volumes of ferrite fractions and higher yield strength at lower austempering temperatures. The nature of the ausferrite microstructure depends on the austempering time and the temperature [23]. At higher austempering temperatures of 420–520 °C, the size of ausferrite increased, and the ausferrite phase formed in the microstructure. Large austenite regions at 620 °C were discrete from each other, and rough ferrite was determined. Therefore, the rise of the austempering temperature caused the ausferrite needles to thicken and increase the ausferrite rate. While the average lath and ausferrite length are approximately identical, they have wide diversity.

The remaining austenite was maintained to absorb the carbon, thereby progressively increasing the carbon content of austenite. Due to the low diffusion rate and fast ferrite formation kinetics at low austempering temperatures, very little carbon was dispersed into austenite. A low carbon diffusion rate could lead to a reduction of carbon-rich and stable austenite. Therefore, the carbon rate was minor at low temperatures. As the austempering temperature raised, more carbon could be emitted to the surrounding austenite; hence it was thought that carbon distribution was rapid in austenite when the isothermal conversion temperature was raised over 380 °C, and carbon enhanced in austenite with the enlargement of ausferrite. XRD patterns of as-cast and austempered samples at various temperatures are represented in Figs. 6–8. The result of XRD established that the basic phases in the samples were mainly ferrite (α), graphite, and ausferrite phases.

3.2. Tensile test

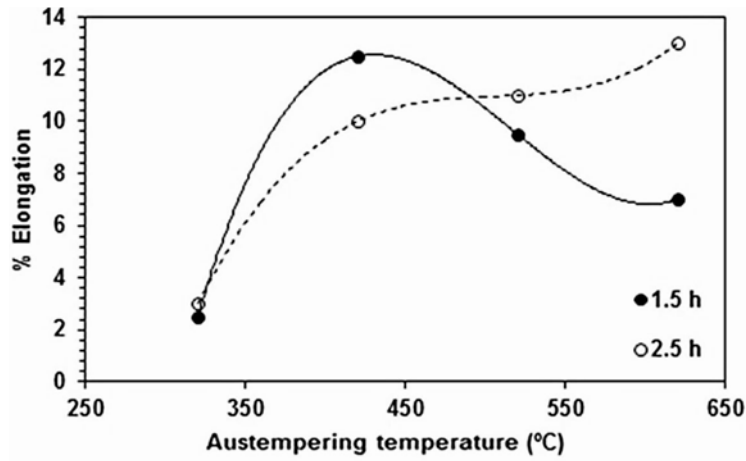Tensile tests of as-cast and austempered samples

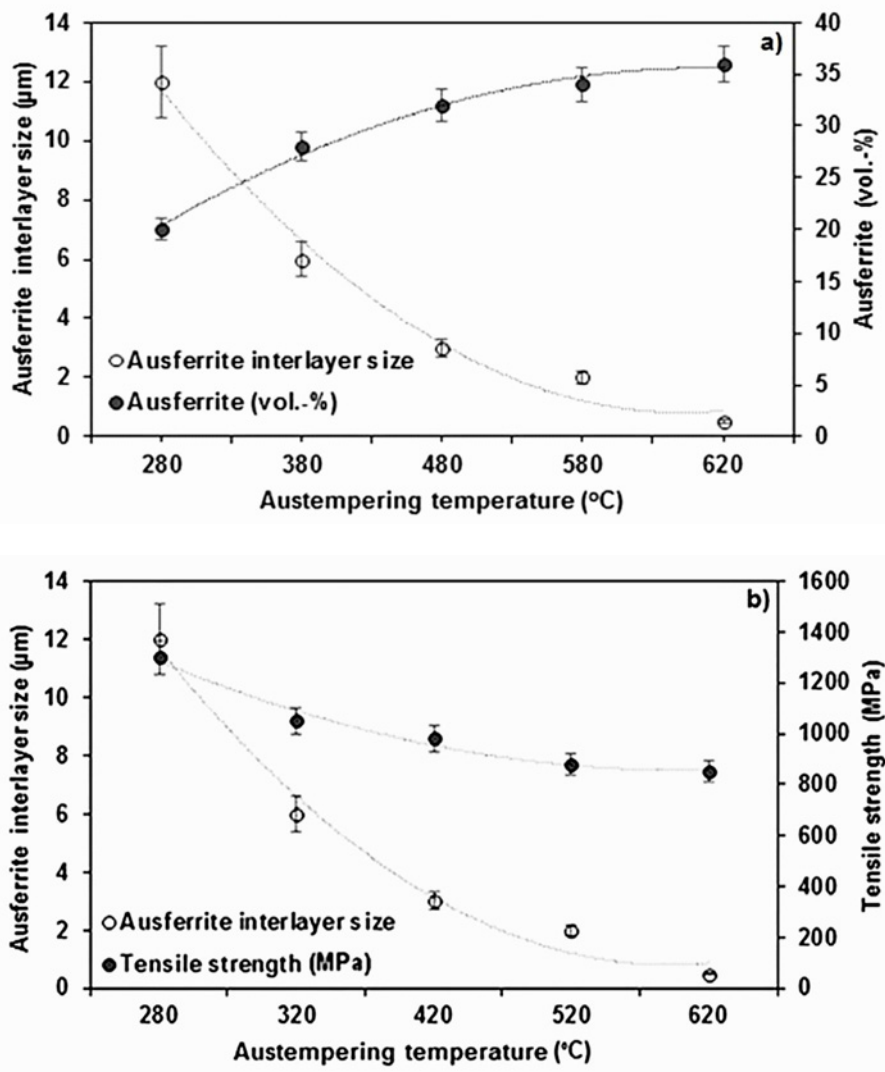Fig. 10. The % elongation results of as-cast and austempered samples.

Fig. 11a,b. Relationship between (a) austempering temperature-ausferrite interlayer size-ausferrite vol.%, (b) austempering temperature-ausferrite interlayer size-tensile strength.

are displayed in Figs. 9 and 10. SSFDCI materials containing 4.3 wt.% Si indicated a fully ferritic structural matrix. The silicon rate induced solid solution strength. Thus, the base profit of such materials was
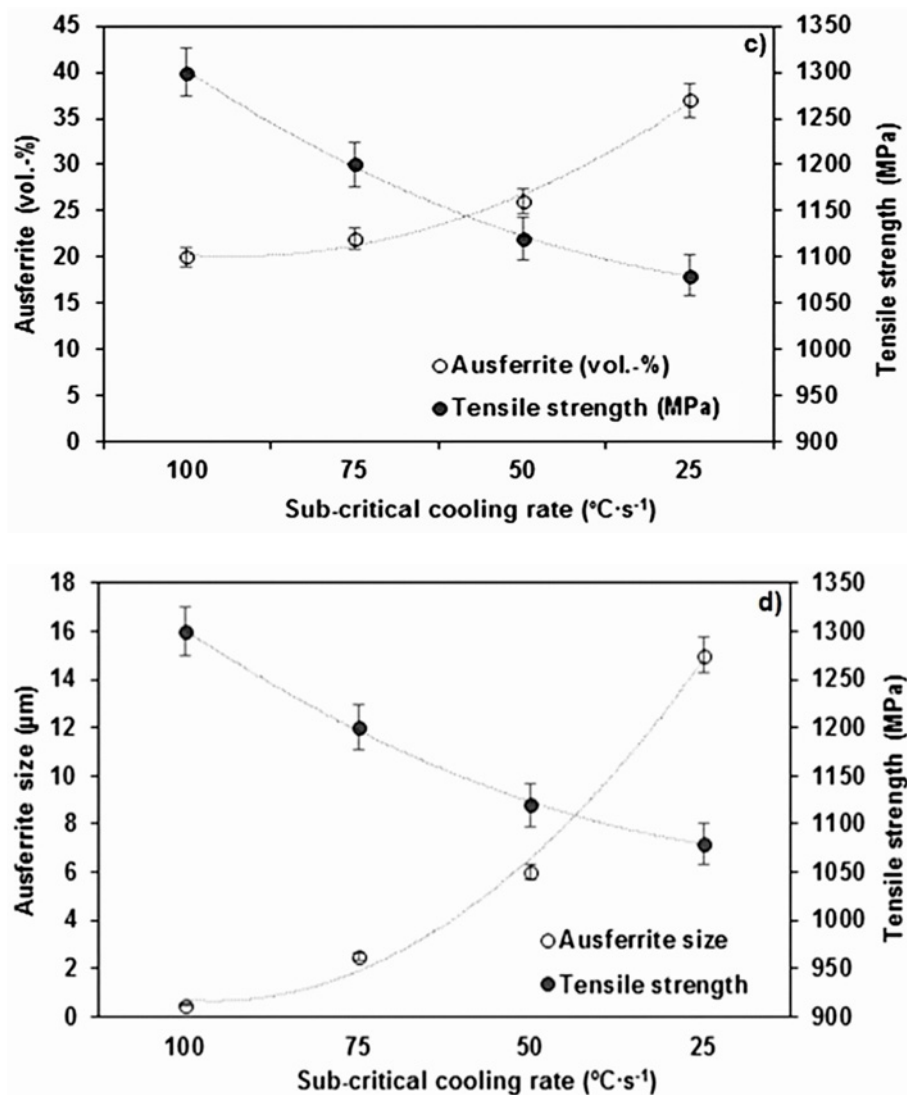
Fig. 11c,d. Relationship between (c) sub-critical diffusion cooling rate-ausferrite volume-tensile strength, (d) ausferrite cooling rate-ausferrite size-tensile strength.

a powerful microstructure. SSFDCI alloys had high strength and ductility features since they were alloyed with 3.2–4.3 wt.% Si [5]. The Si intensity in the microstructure limited iron carbide formation in the as-cast but enhanced the solid solution strengthening properties. SSFDCI comprised a fully ferritic matrix, steadied with a high silicon density [8]. In addition, the increasing silicon wt.% promoted continued eutectic solidification and significantly strengthened the ferritic matrix. The tensile strength of austempering steels was always higher than that of "as-cast" irons [23]. With the increase in austempering temperature, the tensile strength and stiffness decreased, and the elongation percentage increased. It was found that the strength at any step of the discontinuous tempering was rather connected with the phase structure. These analyses show that the strength was mainly dependent on ausferrite dispersion, but the dispersion of grain

size, particle measure, and dislocation concentration were not free parameters [25]. As the amount of the ausferrite phase decreased, the hardness of the ductile iron was reduced. The low austempering temperature exhibited higher strength results than the high temperature. As shown in Fig. 9, the tensile and yield strengths declined sedately as the austempering temperature increased. It was found that elongation and ductility developed. The samples austempered at 280, 320, 420, and 620 °C displayed tensile strength of 900, 1100, 945, and 850 MPa, respectively. The increase in strength with decreasing austempering temperature resulted from refining the microstructure (Figs. 11a–d). The mechanical act of ADI, which was austempered at different temperatures, was formed by different mechanisms. Fine ferrite laths at low temperatures and strain hardening of austenite which was present in large amounts at high temperatures were formed. An
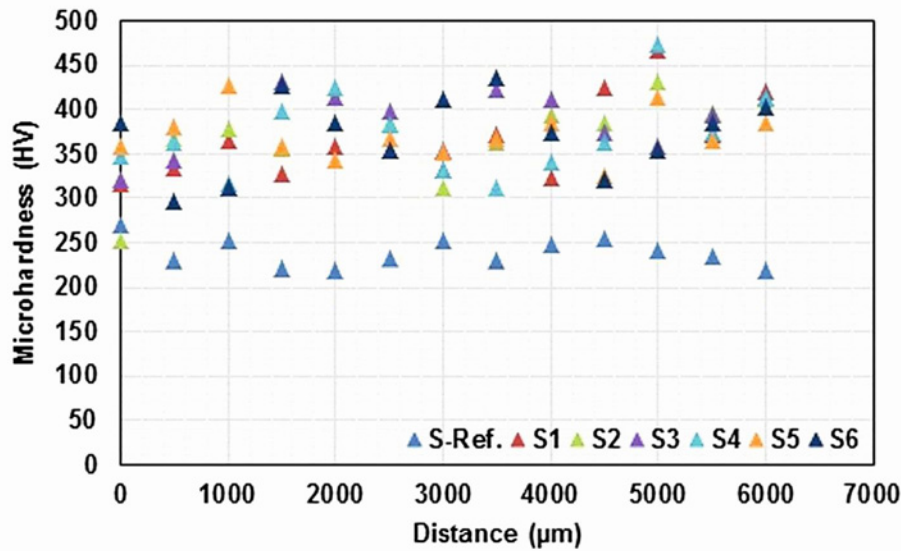
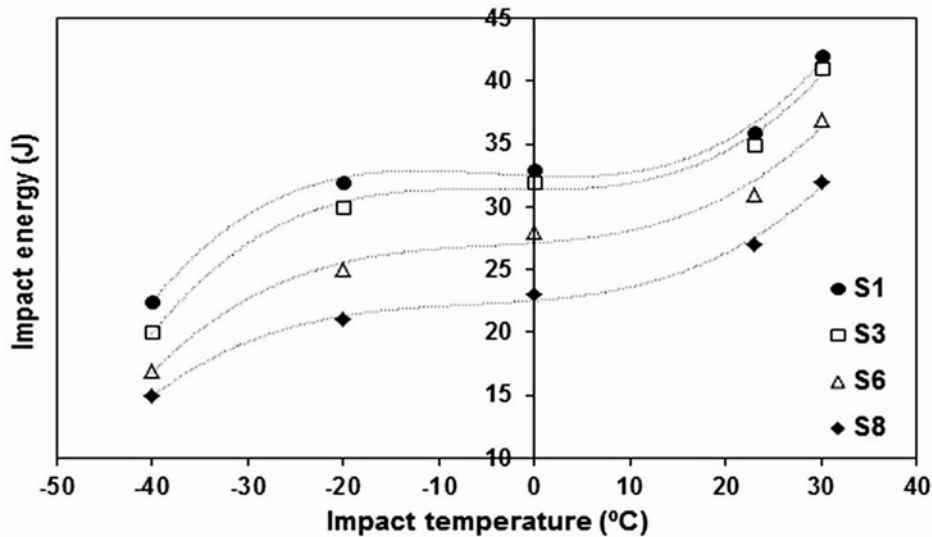Fig. 12. The hardness values of samples.

Fig. 13. The impact test results of samples.

increase in ausferrite size reduced strength and hardness with an extensive rate of austenite (Figs. 11a,b). It was seen that the cooling rate of ausferrite was effective on the austempering temperature effect, such as ausferritic structure and tensile strength (Figs. 11c,d). It is thought that the increase in isothermal holding temperature may form strain-induced martensite, which can form strain deformation during ADIs and may lead to increased strain hardening. On the other hand, the increase in austempering temperature can inspire excess carbon emissions, which provoke an increase in ausferrite size (in vol.%) [23, 24]. Besides, the ausferrite content was increased, reducing the amount of austenite converted. Higher austempering temperatures produced ausferrite and a lower ferrite volume, leading to low yield strength. The morphology of ausferrite changes according to the car-

bon rate of austenite and the austempering temperature.

The hardness values of samples are exhibited in Fig. 12. As the austempering temperature dropped, the hardness increased. Thin ausferrite microstructure formed at low austempering temperatures gave higher hardness. The rough ausferrite microstructure formed at high temperatures had low hardness. The location of austenite was the primary factor. If there was a martensite around austenite, the latter could turn into martensite in the initial tension stages. Therefore, the size, morphology, and spread of austenite became more and more suitable for converting austenite to martensite during plastic deformation as the austempering temperature increased [20–22].

The impact test values of as-cast and austempered samples at different temperatures are shown in Fig. 13.

The ausferrite microstructure of SSFDCI obtained for low austempering temperatures had higher fracture toughness than upper ausferrite microstructures. The austempered upper ausferrite microstructure ductile iron had a higher tensile elongation, which concerned the size and concentration of acicular ferrite and ausferrite. High strength at low austempering temperature ($< 420\,$℃) was related to the formation of high-strength acicular ferrite, which was preponderant in the structure. In ausferritic structures, lower ausferritic microstructures provided better toughness than upper ausferritic microstructures [25, 26]. The rate of ausferrite in the microstructure was a main parameter affecting impact strength (Fig. 13). It was seen that the microstructure of the Ce microalloyed samples having small acicular ferrite austempered at $320\,$℃ and 1.5 h gave impact energy of $\cong 35$ J; however, the increase of the austempering temperature over $380\,$℃ decreased the impact energy under ≤ 30 J for room temperature testing. In addition, the transition temperature of the samples was detected as approximately $-20\,$℃ for all samples tested.

The fracture surfaces of austempered samples are shown in Figs. 14a–c. It was seen that the pit size increased, but the number of pits reduced with the increment in the austempering temperature. During the tensile test, some micro cavities developed initially in the neck area. As the austempering temperature increased, ausferrite morphology changed from thin to rough. Consequently, strength decreased, and ductility increased. These variables reduced the rate of ausferrite laths, expanded the laths, reduced strength and stiffness, and increased ductility.

4. Conclusions

The influence of austempering conditions on the microstructure, hardness, tensile strength, and toughness grades of Ce-La microalloyed solution-strengthened ferritic ductile irons (SSFDCI) was analyzed. The results obtained are as follows:

1. Film-like residual austenite formed at low austempering temperature produced nano-sized ausferrites.

2. For high austempering temperatures, austenite retained in the type of block morphology, producing ausferrite having more than $5\,\mu$m in size.

3. Austempering advanced the mechanical features of Ce-La alloyed samples. The tensile strength increased, and the ductility decremented with the drop in the sub-critical temperature.

4. The fracture mechanism after the tensile test was in the form of a cup and cone, which was an indicator of ductile fracture. The pit size expanded with rising austempering temperature, indicating improved ductility.
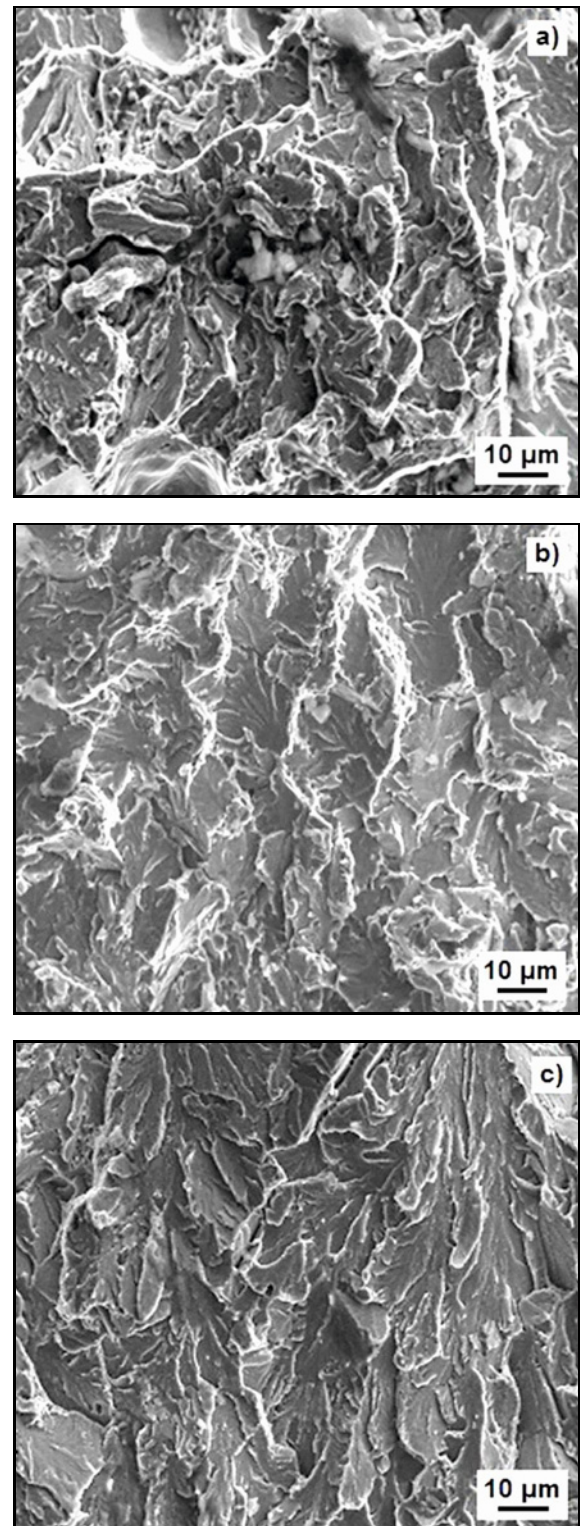

Fig. 14. The fracture surface of austempered samples for (a) 420, (b) 520, and (c) 620 ℃.

5. Maximum tensile strength (1100 MPa) at low austempering temperature (320 ℃) was related to the lower-sized ausferrite.

6. Increase in the sub-critical cooling rate transformed the ausferrite phase and dispersed in the matrix.

7. The presence of Ce-La was homogeneously distributed in the ausferrite.

8. Thinner and larger volumes of ausferrite fractions and higher yield strength were achieved at low austempering temperatures.

Acknowledgement

References

[1] O. Eric, M. Jovanovic, L. Sidjanin, D. Rajnovic, S. Zec, The austempering study of alloyed ductile iron, Mater. Des. 27 (2006) 617–622.
https://doi.org/10.1016/j.matdes.2004.11.028

[2] L. Masud, R. Martinez, S. Simison, R. Boeri, Embrittlement of austempered ductile iron on contact with water–testing under applied potential, J. Mater. Sci. 38 (2003) 2971–2977.
https://doi.org/10.1023/A:1024425727963

[3] A. D. Basso, R. A. Martínez, J. A. Sikora, Influence of austenitising and austempering temperatures on microstructure and properties of dual phase ADI, Mater. Sci. Tech. 23 (2007) 1321–1326.
https://doi.org/10.1179/174328407X236544

[4] D. Li, Z. Zhou, D. Sun, Analysis on the welding heat-affected zone microstructures of austempered ductile iron, J. Mater. Sci. 39 (2004) 7119–7124. https://doi.org/10.1023/B:JMSC.0000047563.46550.e6

[5] A. Basso, R. Martínez, J. Sikora, Influence of chemical composition and holding time on austenite (γ)→ferrite (α) transformation in ductile iron occurring within the intercritical interval, J. Alloy. Compd. 509 (2011) 9884–9889.
https://doi.org/10.1016/j.jallcom.2011.07.069

[6] S. C. Murcia, M. A. Paniagua, E. A. Ossa, Development of as-cast dual matrix structure (DMS) ductile iron, Mater. Sci. Eng. A 566 (2013) 8–15.
https://doi.org/10.1016/j.msea.2012.12.033

[7] A. Alhussein, M. Risbet, A. Bastien, J. P. Chobaut, D. Balloy, J. Favergeon, Influence of silicon and addition elements on the mechanical behavior of ferritic ductile cast iron, Mater. Sci. Eng. A 605 (2014) 222–228.
https://doi.org/10.1016/j.msea.2014.03.057

[8] T. Engelke, A. Esderts, Analytical strength assessments of austempered ductile iron components, Mater. Test. 60 (2018) 940–944.
https://doi.org/10.3139/120.111235

[9] P. P. Rao, S. K. Putatunda, Investigations on the fracture toughness of austempered ductile irons austenitized at different temperatures, Mater. Sci. Eng. A 349 (2003) 136–149.
https://doi.org/10.1016/S0921-5093(02)00633-0

[10] T. Teker, I. S. Dalmis, R. Yilmaz, Effect of heat treatment on the wear behavior of GX200Cr13Ni6WMoMn, Mater. Test. 61 (2019) 441–447.
https://doi.org/10.3139/120.111339

[11] Y. J. Kim, H. Shin, H. Park, J. D. Lim, Investigation into mechanical properties of austempered ductile cast iron (ADI) in accordance with austempering temperature, Mater. Lett. 62 (2008) 357–360.
https://doi.org/10.1016/j.matlet.2007.05.028

[12] L. F. V. Guerra, A. B. Jacuinde, I. Mejia, J. Zuno, C. Maldonado, Effects of boron addition and austempering time on microstructure, hardness and tensile properties of ductile irons, Mater. Sci. Eng. A 648 (2015) 193–201. https://doi.org/10.1016/j.msea.2015.09.066

[13] T. Giętka, T. Szykowny, Microstructure and mechanical properties of ADI depending on austenitization methods and parameters, Arch. Foundry Eng. 12 (2012) 19–24.
https://doi.org/10.2478/v10266-012-0029-6

[14] J. F. Dias, G. O. Ribeiro, D. J. Carmo, J. J. Vilela, The effect of reducing the austempering time on the fatigue properties of austempered ductile iron, Mater. Sci. Eng. A 556 (2012) 408–413.
https://doi.org/10.1016/j.msea.2012.07.005

[15] T. Kobayashi, H. Yamamoto, Development of high toughness in austempered type ductile cast iron and evaluation of its properties, Metall. Trans. A 19 (1998) 319–327. https://doi.org/10.1007/BF02652541

[16] K. Soivio, Austempering experiments of production grade silicon solution strengthened ductile iron, Mater. Sci. Forum 925 (2018) 239–245. https://doi.org/10.4028/www.scientific.net/MSF.925.239

[17] ASTM A571M, Standard specification for austenitic ductile iron castings for pressure-containing parts suitable for low-temperature service, ASTM International, West Conshohocken, PA, USA, 2002.

[18] ASTM E8M–04, Standard test methods for tension testing of metallic materials, ASTM International, West Conshohocken, PA, USA, 2004.

[19] ASTM E23–06, Standard test methods for notched bar impact testing of metallic materials. ASTM International, West Conshohocken, PA, USA, 2000.

[20] S. Panneerselvam, S. K. Putatunda, R. Gundlach, J. Boileau, An investigation on the stability of austenite in austempered ductile cast iron (ADI), Mater. Sci. Eng. A 694 (2017) 72–80
https://doi.org/10.1016/j.msea.2014.12.038

[21] P. Sellamuthu, D. G. Harris Samuel, D. Dinakaran, V. P. Premkumar, Z. Li, S. Seetharaman, Austempered ductile iron (ADI): Influence of austempering temperature on microstructure, mechanical and wear properties and energy consumption, Metals 8 (2018) 53–64.
https://doi.org/10.3390/met8010053

[22] J. L. Garin, R. L. Mannheim, Strain-induced martensite in ADI alloys, J. Mater. Process. Technol. 143–144 (2003) 347–351.
https://doi.org/10.1016/S0924-0136(03)00452-7

[23] S. Panneerselvam, C. J. Martis, S. K. Putatunda, J. M. Boileau, An investigation on the stability of austenite in austempered ductile cast iron (ADI), Mater. Sci. Eng. A 626 (2015) 237–246.
https://doi.org/10.1016/j.msea.2014.12.038

[24] P. P. Rao, S. K. Putatunda, Comparative study of fracture toughness of austempered ductile irons with upper and lower ausferrite microstructures, Mater.

Sci. Technol. 14 (1998) 1257–1265.
https://doi.org/10.1179/mst.1998.14.12.1257

[25] M. Ramadan, N. Fathy, Influence of semi-solid isothermal heat treatment on microstructure and mechanical properties of ductile cast iron, J. Min. Mater. Charac. Eng. 2 (2014) 26–31.
https://doi.org/10.4236/jmmce.2014.21005

[26] S. K. Putatunda, Development of austempered ductile cast iron (ADI) with simultaneous high yield strength and fracture toughness by a novel two-step austempering process, Mater. Sci. Eng. A 315 (2001) 70–80.
https://doi.org/10.1016/S0921-5093(01)01210-2